Microscopic characterisation and chemical analysis of modified asphalt-grout ITZ in SFP material using silane coupling agent

Liu, Xiaoyu; Ni, Botao; Wu, Kuanghuai; Li, Yi; Yue, Yunpeng; Cai, Xu; Ren, Fengming

DOI
10.1080/10298436.2025.2503399

Publication date
2025

Document Version
Final published version

Published in
International Journal of Pavement Engineering

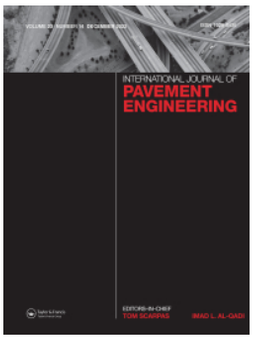

International Journal of Pavement Engineering

ISSN: 1029-8436 (Print) 1477-268X (Online) Journal homepage: www.tandfonline.com/journals/gpav20

Microscopic characterisation and chemical analysis of modified asphalt-grout ITZ in SFP material using silane coupling agent

Xiaoyu Liu, Botao Ni, Kuanghuai Wu, Yi Li, Yunpeng Yue, Xu Cai & Fengming Ren

To cite this article: Xiaoyu Liu, Botao Ni, Kuanghuai Wu, Yi Li, Yunpeng Yue, Xu Cai & Fengming Ren (2025) Microscopic characterisation and chemical analysis of modified asphalt-grout ITZ in SFP material using silane coupling agent, International Journal of Pavement Engineering, 26:1, 2503399, DOI: 10.1080/10298436.2025.2503399

To link to this article: https://doi.org/10.1080/10298436.2025.2503399

Published online: 03 Jun 2025.

INTERNATIONAL JOURNAL OF PAVEMENT ENGINEERING
2025, VOL. 26, NO. 1, 2503399
https://doi.org/10.1080/10298436.2025.2503399

Microscopic characterisation and chemical analysis of modified asphalt-grout ITZ in SFP material using silane coupling agent

Xiaoyu Liu [a], Botao Ni[b], Kuanghuai Wu[a], Yi Li[c], Yunpeng Yue[a], Xu Cai [a] and Fengming Ren[a]

[a]School of Civil Engineering and Transportation, Guangzhou University, Guangzhou, People's Republic of China; [b]Yong Fu Construction Engineering Group Co., Ltd., Fuzhou, People's Republic of China; [c]Section of Pavement Engineering, Faculty of Civil Engineering & Geosciences, Delft University of Technology, Delft, The Netherlands

ABSTRACT

Semi-flexible pavement (SFP) is a composite material comprising porous asphalt and cementitious grout. Its asphalt-grout interfacial transition zones (ITZ) are prone to cracking. While interfacial modifiers can improve ITZ crack resistance, their effects on microscopic morphology and chemical composition remain unclear, limiting the understanding of mechanisms influencing ITZ performance and the optimised use of modifiers. To achieve this challenge, the study characterised the microscopic morphology and chemical composition of the asphalt-grout ITZ in SFP, particularly those modified by immersion in a silane coupling agent solution. The asphalt-grout ITZ in SFP material is analyzed using a series of micromechanics techniques, including scanning electron microscopy (SEM) for microscopic morphology, energy dispersive spectrum analysis (EDS) for chemical components, X-ray diffraction (XRD) for phase composition, and Fourier-transform infrared spectroscopy (FTIR) for chemical bond information. The results indicate that an interfacial modifier can effectively enhance the microscopic bonding between asphalt and grout material, reducing the likelihood of tiny cracks between these two phases. The asphalt-grout ITZ exhibits a distinct double-layer structure, with altered morphology compared to the bulk material, including hexagonal calcium hydroxide crystals aggregation, which is more prone to cracking than hydrated calcium silicate (C–S-H) gel. Element distribution at the enhanced interface is more continuous, with synchronous enrichment. These findings provide insights into proactive strategies for improving crack resistance at asphalt-grout ITZ, thereby strengthening the road performance of SFP materials.

ARTICLE HISTORY
Received 6 January 2025
Accepted 3 May 2025

KEYWORDS
Semi-flexible Pavement (SFP); asphalt-grout interfacial transition zone (ITZ); interfacial modifier; silane coupling agent; microscopic morphology; chemical components

1. Introduction

Semi-flexible pavements (SFP) have garnered increasing attention as a promising alternative to traditional pavement materials due to their superior mechanical properties (Xu *et al.* 2021, Khan *et al.* 2022, Zarei *et al.* 2022a), including enhanced rutting resistance and load-bearing capacity (Disfani *et al.* 2020, Sui *et al.* 2024, Tan *et al.* 2024). SFP consists of porous asphalt mixtures (PAM) combined with cementitious grout substances, creating a composite material that leverages the strengths of both asphalt and cement-based materials (Saboo *et al.* 2019, Fang *et al.* 2022, Ling *et al.* 2022) (Figure 1). However, one of the primary challenges in the development and performance of SFP lies in the asphalt-grout interfacial transition zone (ITZ) (Wu *et al.* 2021, Liu *et al.* 2025c), where the distinct properties of the asphalt and cementitious grout materials meet with each other (Zhang *et al.* 2024b). This region is highly susceptible to cracking due to the inherent differences in their mechanical behaviours, which negatively impact the overall performance and longevity of the pavement (Gong *et al.* 2019, Ling *et al.* 2024). Asphalt-grout-based SFP is a novel structural form that differs from traditional flexible or rigid pavements by integrating a flexible asphalt skeleton with a rigid cementitious filler (Cheng *et al.* 2023, Liu *et al.* 2025b). This dual-phase structure provides a balance of flexibility and strength, making it well-suited for heavy-load and high-stress applications such as ports and intersections (Liu *et al.* 2025a). Compared with conventional asphalt or concrete pavements, it offers improved fatigue resistance, higher deformation tolerance, and better long-term durability (Song *et al.* 2024).

The presence of ITZs in SFP is a critical cause of material failure (Raza and Sharma 2024), as these regions are highly susceptible to crack initiation and propagation (Zarei *et al.* 2022b, Khan *et al.* 2024, Zhang *et al.* 2024a). In particular, asphalt-grout interfaces are highly susceptible to cracking in real engineering applications of SFPs (Liu *et al.* 2023, Chen *et al.* 2024). Interfacial modifiers, such as silane coupling agents, have demonstrated the potential to improve crack resistance at the macro level by enhancing the bonding between asphalt and grout materials (Liu *et al.* 2023, Wang *et al.* 2024). However, the complex, multi-phase nature of the asphalt-grout interface makes it challenging to comprehend the underlying mechanisms governing its behaviour fully (Cai *et al.* 2021, Hu *et al.* 2023), particularly in terms of bonding strength, crack propagation resistance, and the role of microstructural changes at the ITZ (Li *et al.* 2020, Li *et al.* 2022).

This knowledge gap limits the optimisation of the SFP design (Davoodi *et al.* 2022, Wang *et al.* 2022), particularly

CONTACT Kuanghuai Wu wukuanghuai@163.com; Fengming Ren rfm@gzhu.edu.cn

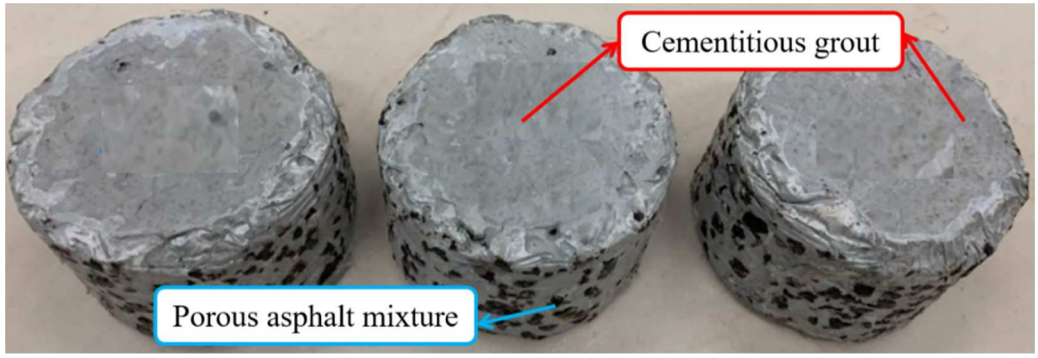

Figure 1. Sample of conventional SFP (101.6 ± 0.2mm × 63.5m ± 1.3 mm).

given that the long-term durability and performance of SFP materials depend critically on the properties of the asphalt-grout interface (Fan *et al.* 2024, Songqiang *et al.* 2024). While some research has addressed the macro-mechanical properties of SFPs and the general effects of interfacial modifiers, insufficient attention has been paid to the ITZ's microscopic morphology and chemical composition before and after modification (Ferreira *et al.* 2022). The microstructural evolution of SFP before and after reinforcement remains insufficiently explored. Although macro-scale strength tests can reveal the bonding properties of the asphalt-grout ITZ in SFP after the interfacial modifier. However, the precise mechanisms of how these modifiers interact with the materials at the interface, and how they influence microstructural properties such as crystal formation, bond continuity, and crack resistance, remain unclear (Tian *et al.* 2021). Addressing these research gaps is crucial for developing a more comprehensive understanding of the asphalt-grout ITZ and optimising interfacial modifiers' use to enhance the crack resistance and overall performance of SFPs under real-world conditions (Sun *et al.* 2015, Wang *et al.* 2021, Jiang *et al.* 2022). Therefore, further investigation is required to elucidate the damage mechanisms occurring at the ITZ and their impact on SFP performance through the application of micromechanics techniques.

This study aims to characterise the microscopic morphology and chemical composition of the asphalt-grout ITZ in SFP with the interfacial modifier. The SFP is modified by immersion in a silane coupling agent solution to improve crack resistance at asphalt-grout interfaces, thereby enhancing the road performance of SFP materials. Figure 2 illustrates the flowchart of the laboratory experimental procedure. This paper presents an overview of the micromechanics test using SFP materials through scanning electron microscopy (SEM) for microscopic morphology, energy dispersive spectrum analysis (EDS) for chemical components, X-ray diffraction (XRD) for phase composition, and Fourier-transform infrared spectroscopy (FTIR) for chemical bond information is presented, along with the introduction of the three types of grout materials with different strengths and the interfacial modifier method. These findings provide insights into proactive strategies for improving crack resistance at asphalt-grout ITZ, thereby strengthening the road performance of SFP materials.

2. Materials and methods

2.1. Materials

2.1.1. Asphalt and aggregate

SBS-modified asphalt was applied to form SFP in this study. The SBS-modified asphalt parameters are listed in Table 1. Natural diabase was utilised as the coarse aggregate (Table 2). The particle size distribution of the PAM specimens is as follows: aggregates with a size range of 9.5-13.6 mm account for 63.1%, while those in the ranges of 4.75–9.5 mm and 2.36–4.75 mm constitute 24.9% and 8.5%, respectively. Mineral powder comprises 3.5% of the mixture, and the bitumen-to-aggregate ratio is 3.6%. The void ratio of the PAM specimens was determined using the Volume Method, as specified in Chinese standard JT/T E20-2017 (China 2011), and ranged from 28%–30%.

2.1.2. Grout materials

Three distinct kinds of grout with varying strengths were used, Table 3 displays the specs for these materials. The grout materials GM-40, GM-60, and GM-70 had water-binder ratios of 0.32, 0.30, and 0.27, respectively. Different grout materials' compressive, flexural, and tensile strengths were tested according to the Chinese standard JTG 3420–2020 (China 2020). The cement-based grout material was prepared using a small laboratory cement mortar mixer and then poured into the PAM specimens. During the pouring process of GM-60 and GM-70 grout materials, a small vibration table was used to assist the grouting.

2.2. Interfacial modifier method

Prior studies (Liu *et al.* 2023) have proved that grouting PAM specimens after treating them with a silane coupling agent solution can improve the mechanical characteristics of the composite interface in SFP materials. In this study, the silane coupling agent KH-570 was used to immerse the PAM specimens. The agent of KH-570 is a colourless, transparent liquid with a chromatographic purity of 98%. It has a density of 1.02–1.06 g/cm^3. This agent was chosen to enhance the features of the asphalt-grout interface. An immersing solution was made comprised of 72% methanol, 20% silane coupling agent, and 8% water. The PAM specimens were immersed in the interfacial modifier solution at a temperature of 26°C for

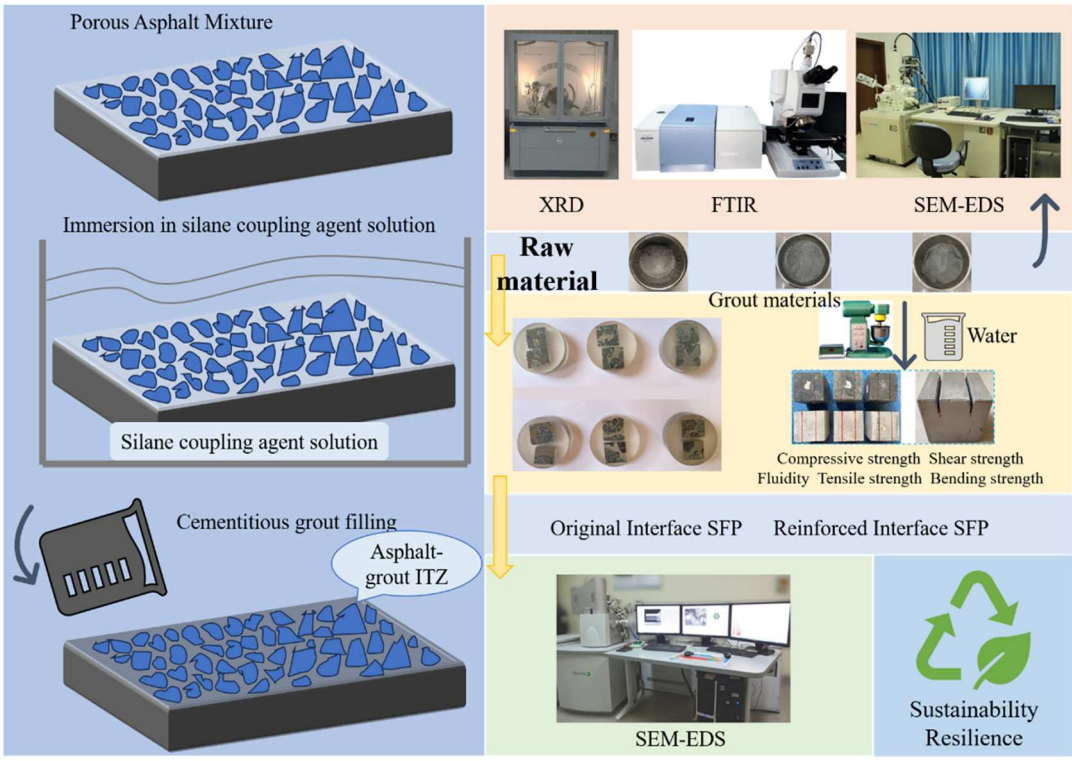

Figure 2. Flowchart of the laboratory experimental procedure.

1 hour. Table 4 lists the types of laboratory experiment cases. Note that all the SFP specimens were placed in a standard curing box to cure for up to 28 days before microscopic tests.

2.3. Experimental methods

2.3.1. Uniaxial penetration test

The uniaxial penetration test was employed to measure the shear strength of asphalt specimens, to compare the mechanical enhancement of SCA on the ITZ in SFP materials, a uniaxial penetration test was conducted to measure the shear strength of asphalt specimens, offering realistic reflection of actual loading conditions (Yang *et al.* 2011). The test utilised cylindrical specimens with φ100 mm × 100 mm dimensions, consistent with those used in uniaxial compression tests. Before testing, the specimens were conditioned in a 60°C oven for 6 hours and then loaded to failure at a constant rate of 1 mm/min. An indenter with a diameter of 28.5 mm was employed. The uniaxial penetration strength, which represents the shear strength of the SFP specimens, is calculated using the following equation:

$$\sigma_P = \frac{p}{A} \tag{1}$$

where σ_P is the uniaxial penetration strength, P is the peak force during loading, and A is the indenter area. Finally, by combining the results of the uniaxial penetration test with those of the uniaxial penetration test and unconfined compressive strength measurements, the cohesion C and internal friction angle φ of the SFP specimens can be determined (Su *et al.* 2008).

2.3.2. Pull-off test

A pull-off test was conducted to assess the macroscopic adhesion performance of the SFP system. Diabase, selected as a representative acidic aggregate, was used to investigate the interfacial bonding strength between the asphalt film and the grout material, both before and following interfacial modification. The SBS-modified asphalt was preheated at 165 °C for 2 hours before being uniformly applied to the upper surfaces of the aggregate specimens. Subsequently, the specimens were reheated at 165 °C for an additional 20 minutes to ensure consistent asphalt distribution. After moulding,

Table 1. Specifications of the SBS-modified asphalt.

Properties	Technical requirements	Experiment results
Ductility @5°C and 5 cm/min (cm)	>20	32.0
Segregation (softening point) @163°C and 48 h (°C)	≤2.5	1
Penetration @25°C,100 g, and 5 s (0.1 mm)	40–60	54.4
Elastic recovery ratio @25°C (%)	≥90	95.0
Penetration index	≥0	0.06
Softening point R&B (°C)	>70	88.5
Viscosity @135°C (pa.s)	≤3.0	2.36

Note: The asphalt was produced by Shell Xinyue (Foshan) Asphalt Co., Ltd.

Table 2. Specifications of the natural diabase.

Properties	13.2-9.5	9.5-4.75	4.75–2.36	Mineral powder
Apparent specific gravity (g/cm^3)	2.946	2.964	2.934	2.84
Water absorption (%)	0.749	0.982	0.724	-
Los Angeles wear (%)	17.10	-	-	-
Crushing value (%)	18.15	-	-	-

Table 3. Specifications of the grout materials.

Materials	Compressive strength (28 d) (MPa)	Flexural strength (28 d) (MPa)	Tensile strength (MPa)	Fluidity (s)
GM-40	36.88	8.30	1.11	10
GM-60	57.02	10.30	2.02	16
GM-70	70.00	11.90	1.19	11

Note: Sobute New Materials Co., Ltd., Beijing Sino-Sina Building Technology Co., Ltd., and Zhejiang Weihua New Building Materials Co., Ltd. manufactured GM-40, GM-60, and GM-70 grout materials, respectively.

Table 4. Specifications for the laboratory experiment case.

Case	Type	Grout materials	Immersion time
1	Original interface	GM-40	0 h
2		GM-60	0 h
3		GM-70	0 h
4	Reinforced interface	GM-40	1 h
5		GM-60	1 h
6		GM-70	1 h

the samples were cured for 28 days to allow full development of grout strength. Tensile test fixtures were installed on the specimens after curing, and the pull-off test was then conducted by standard procedures.

2.3.3. X-ray diffraction (XRD) test

X-ray Diffraction (XRD) analysis (Anton Paar, TTK600) was conducted to investigate the phase composition of the grout materials and the chemical composition of the hydration products. The unhydrated samples were prepared according to specifications and placed on a glass slide. The hydrated samples were cured to 28 d and then ground into powder. For X-ray diffraction mineral analysis, 5 g of the powdered samples was used for mineral analysis. The diffraction was performed using CuKα radiation, with a voltage of 40 kV and a current of 40 mA. The diffraction angle ranged from 5°–80°, with a step length of 2°/min, utilising a Cu target.

2.3.4. Fourier-transform infrared spectroscopy (FTIR) test

Fourier-transform infrared spectroscopy (FTIR) (Bruker, Tensor II + Hyperion 2000) was used to analyze the chemical bond information of the grout material. This technique was employed to examine both the raw materials and the hydration products of the grout materials. The screened powder sample was placed in a vacuum drying oven and dried at 50°C for 24 hours. Subsequently, 1 mg of the dried powder was mixed with 100 mg of potassium bromide and pressed into flakes for analysis. The measurement range was set from 400–4000 cm^{-1}.

2.3.5. Scanning electron microscope (SEM) test

SEM-EDS testing provides detailed insight into the microscopic morphology and chemical composition of the asphalt-grout ITZ of SFP, including its elemental composition, which is particularly effective for examining composite interfaces. SEM analysis (JEM-2100F) was performed using accelerated electron scanning at 20 kV on gold-plated samples. This test examined the microscopic morphology of the asphalt-grout ITZ in SFP materials after interface modification, as illustrated in Figure 3. For this analysis, the surface of the SFP sample was sectioned to create small specimens of the ITZ, each with a size of approximately 1 cm × 1 cm × 0.5 cm. The specimens were then embedded in epoxy resin and polished for observation. A low-speed diamond saw was employed to minimise mechanical stress and thermal damage during the pre-processing stage. The sectioned specimens were then embedded in epoxy resin to provide structural support for subsequent preparation. After curing, the embedded

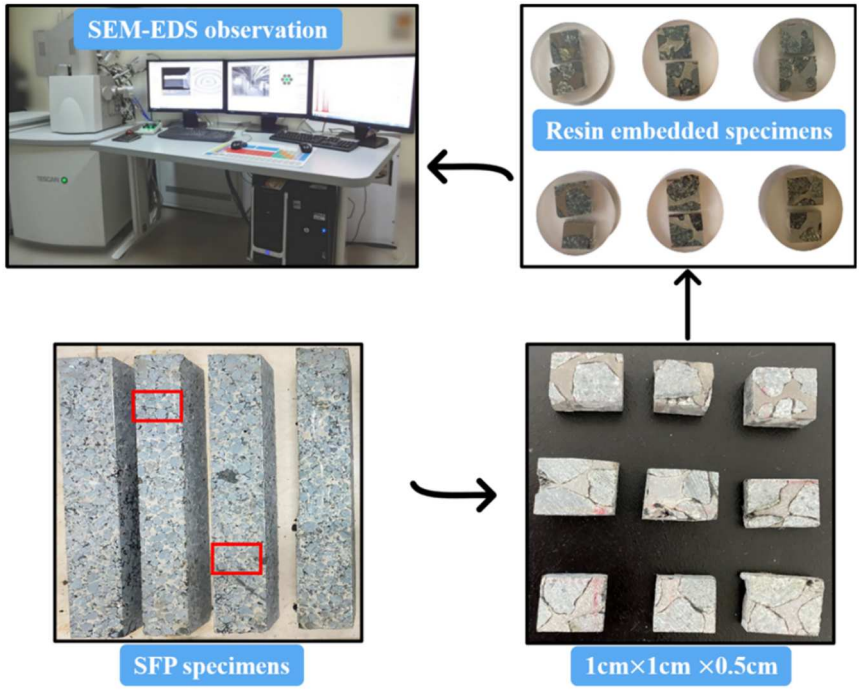

Figure 3. The pre-process and the sample result for the SEM-EDS test.

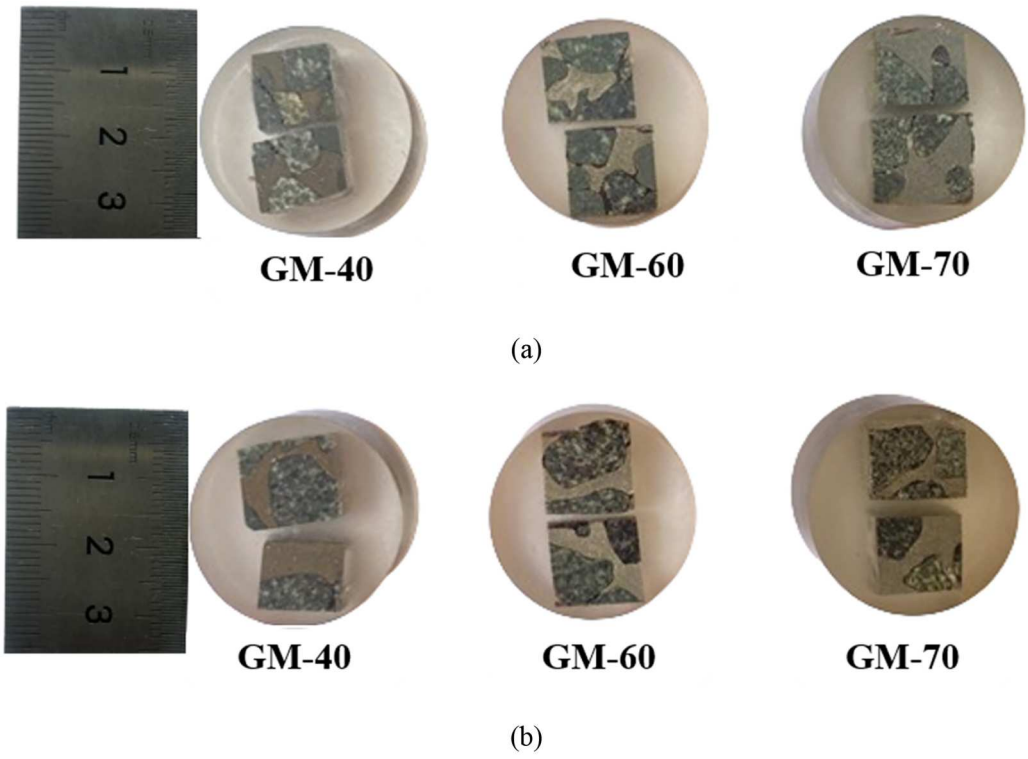

Figure 4. Specimens used for EDS testing of asphalt-grout ITZ in (a) original interface and (b) reinforced interface.

specimens were progressively polished using finer abrasives to avoid dislodging or damaging the delicate ITZ structure. Lubricants were consistently applied during polishing to reduce frictional heat and prevent thermal deformation. The prepared specimens were finally subjected to microscopic observation, as illustrated in Figure 4.

2.3.6. Energy dispersive spectrum (EDS) test

In this study, SEM is mainly suitable for micro-morphological analysis, and to characterise ITZ more precisely, EDS was performed in SEM specimens by line scanning. EDS analysis (Tescan LYRA 3 XNU) was conducted using accelerated electron scanning at 2 kV on samples without gold-plating pretreatment. The sample was subsequently cleaned to obtain the final specimen. Additionally, a line-mode scan was performed in EDS with a dwell time of 0.1 s to measure the elemental concentration across the asphalt-grout ITZ phase.

3. Results

3.1. Marcoscale and mesoscale analysis

3.1.1. Uniaxial penetration test

The shear strength of SFP specimens formed with different grout materials is presented in Table 4. The average uniaxial penetration strength of three SFP specimens was used to determine the final result. As shown in Table 5, the uniaxial penetration strength of the SFP specimens increased after interface modification. Cohesion and internal friction angle serve as indicators of the adhesion strength between the asphalt and grouting material. Higher values of these parameters reflect improved adhesion at the asphalt-grout interface in SFP materials. It is suggested that the interface plays a dominant role in load transfer within the composite system, particularly under shear or penetration loading conditions. Interface modification enhances the adhesive properties of the asphalt, resulting in increased cohesion and stronger intermolecular forces. The use of a silane coupling agent introduces chemical bonds such as Si–O–Si at the interface, promoting better compatibility between the hydrophobic asphalt and the hydrophilic grout. This improvement manifests as the superior mechanical performance of the modified SFP material on the macroscopic scale. The enhanced adhesion reduces the ITZ between the asphalt and grouting material at the microscopic scale. This microstructural refinement can also contribute to long-term durability and reduced susceptibility to moisture damage, which are critical for pavement performance.

3.1.2. Pull-off test

Table 6 presents the pull-off test results for specimens incorporating grout materials of varying strengths, both before and after asphalt surface treatment with a silane coupling agent. The data indicate that immersion in the silane solution significantly enhanced the interfacial bonding strength, with

Table 5. Results of uniaxial penetration test for SFP formed with three types of grouting materials.

Interface type	Grout type	σ_P (MPa)	C (MPa)	φ(°)
Original interface	GM-40	5.08	0.40	26.13
	GM-60	6.46	0.65	32.19
	GM-70	7.26	2.69	12.41
Reinforced interface	GM-40	7.28	0.50	38.59
	GM-60	7.97	1.15	31.91
	GM-70	7.73	4.16	24.51

Table 6. Results of pull-out test for SFP formed with three types of grouting materials.

Interface type	Grout type	Tensile strength (kPa)
Original interface	GM-40	178.45
	GM-60	161.74
	GM-70	243.84
Reinforced interface	GM-40	448.48
	GM-60	429.66
	GM-70	434.59

the tensile strength increasing from approximately 200 kPa to nearly 400 kPa, representing a maximum improvement of 165.6%. This finding demonstrates that silane coupling agent treatment effectively enhances the adhesion capacity at the asphalt – grout interface in SFP materials.

3.2. Microscale analysis of grout materials

3.2.1. XRD test

The XRD results of three grout materials are illustrated in Figure 5. Three types of cement-based grouts exhibited the same diffraction peaks before hydration, indicating the presence of fundamental substances in the cement matrix. Research shows that SiO_2 can react with the hydration product $Ca(OH)_2$ to form calcium silicate hydrate (C–S–H) gel, effectively filling the internal pores of the cement matrix and refining pore sizes (Lin *et al.*, 2011). Additionally, calcium carbonate whiskers possess both fibrous and particulate properties, allowing them to create a bridging effect within the cement matrix. This promotes bonding between the components and forms a dense, networked flocculent structure. Therefore, the incorporation of SiO_2 and calcium carbonate whiskers into cement mortar can significantly enhance its strength, providing a rationale for the high strength of GM-70 grout.

3.2.2. SEM test

Figure 6 shows the microscopic morphology of the three grout materials after 28 days of standard curing. GM-40 shows a greater presence of spherical particles (Figure 8), identified as fly ash, which enhances its fluidity and accelerates SFP grouting (Montgomery *et al.* 1981). The presence of fibres is obvious in the GM-70, which corresponds to the high tensile strength. At this magnification, GM-70 is still the densest, which is consistent with the highest compressive strength of the three materials. In contrast, the surface of GM-60 appears loose and porous, indicating lower density compared to GM-70, which correlates with its reduced compressive strength.

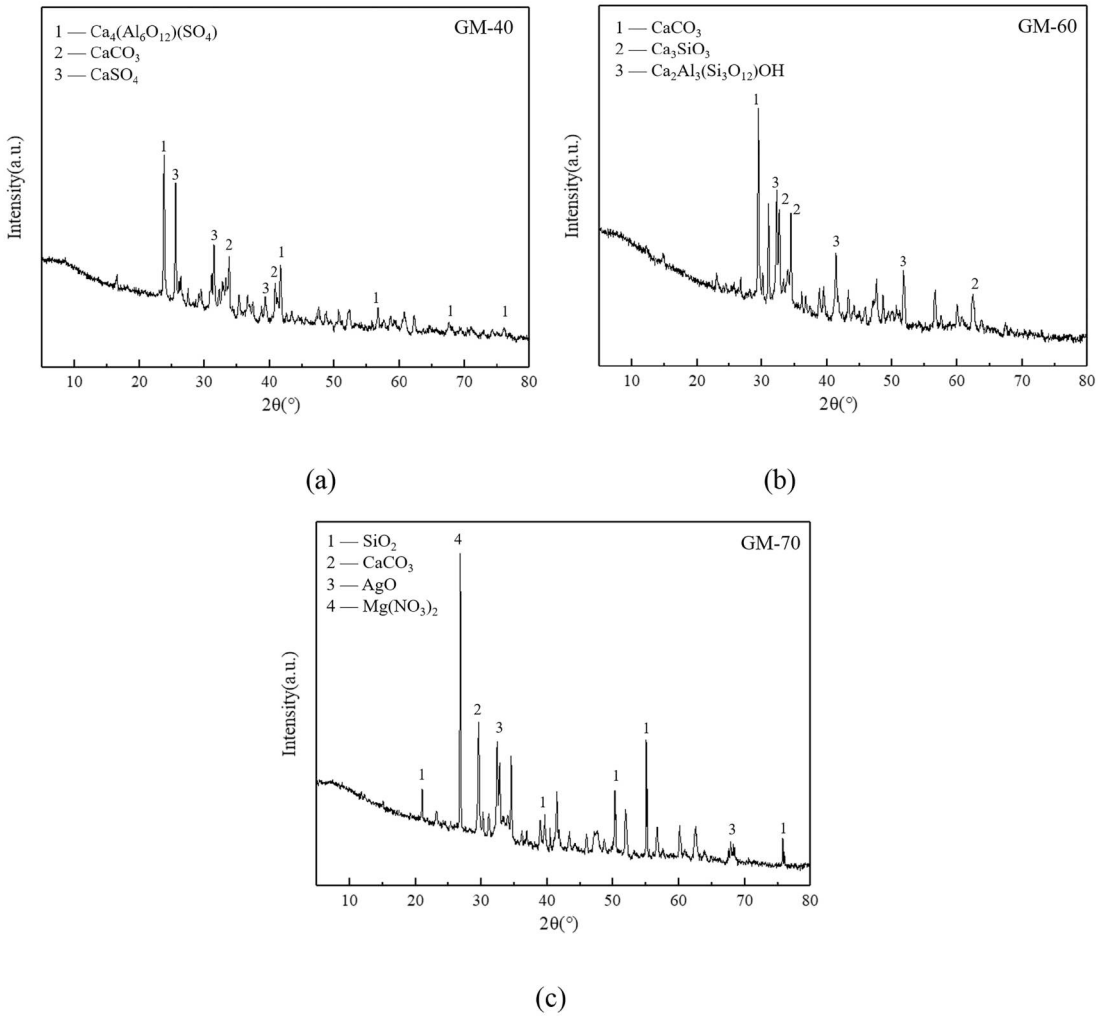

Figure 5. XRD pattern of the (a) GM-40, (b) GM-60, and (c) GM-70 grout materials.

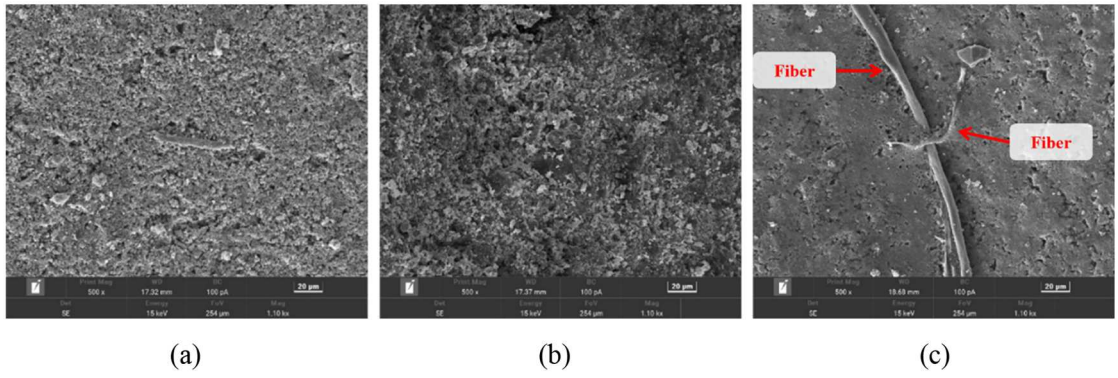

Figure 6. Microscopic morphology of the (a) GM-40, (b) GM-60, and (c) GM-70 grout materials.

3.3. Microscopic morphology analysis

The SEM images of the asphalt-grout ITZ phase in SFP are shown in Figure 7. Since the electrical conductivity of SFP is weak, the sample was pre-treated with gold plating before observation. Figure 7 shows SEM images containing all three phases, *i.e.* aggregate, asphalt, and grout. While the asphalt phase is distinguishable, the aggregate and grout phases are similar in morphology. Obvious cracks were observed at the asphalt-grout interface, and bright bands appeared on both the grout and asphalt sides. This shows that the asphalt-grout interface is an organic–inorganic composite interface with a double-layer structure. The reason is that diffusion

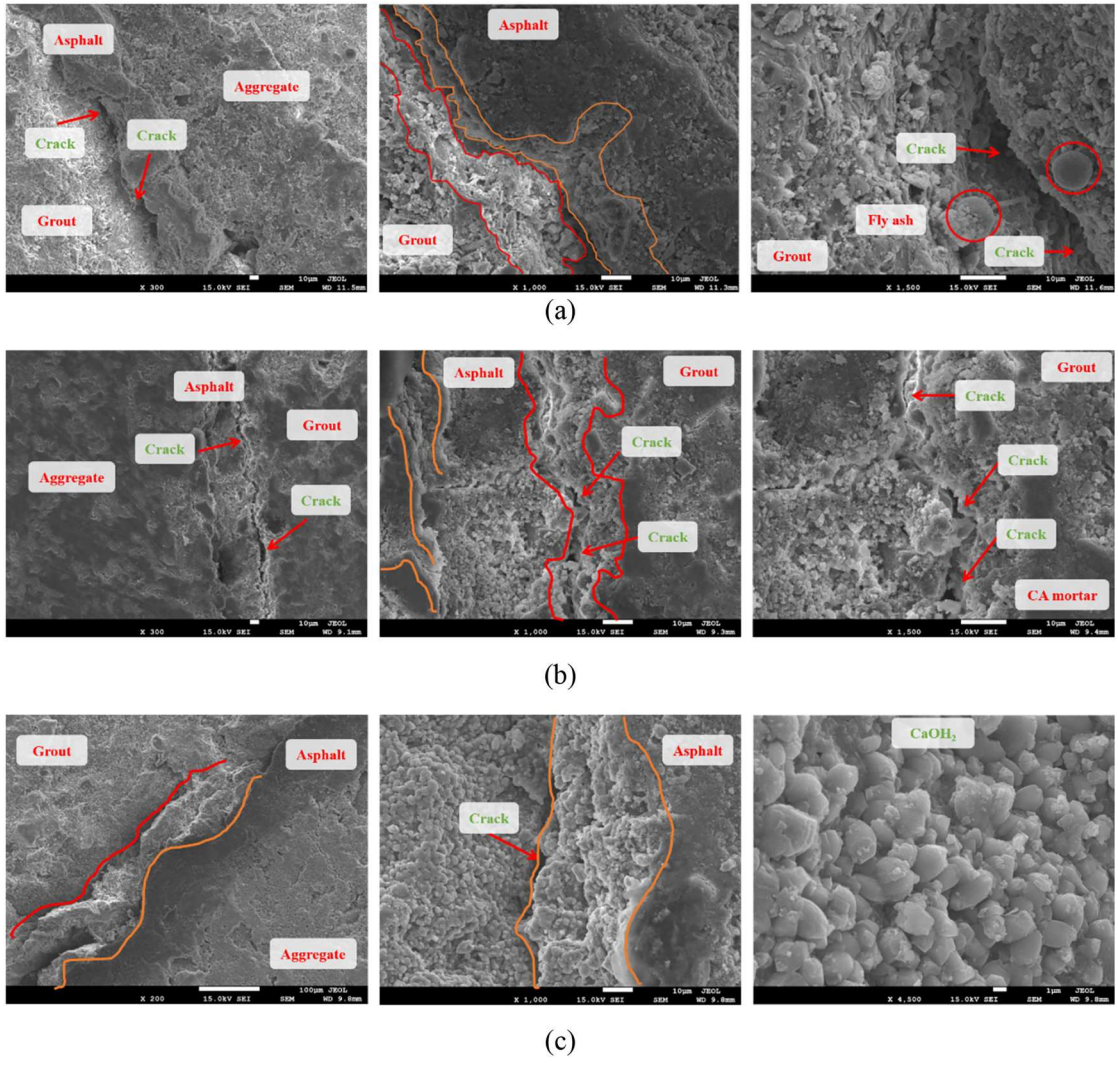

Figure 7. Microscopic morphology of the original interface between asphalt and (a) GM-40, (b) GM-60, and (c) GM-70 grout materials in SFP. The red and yellow areas indicate the ITZ is close to the grout material side and the asphalt side, respectively.

occurs between the asphalt and grout materials. The microscopic morphology of the bright band is significantly different from that of the area far from the interface, indicating that there is material aggregation at the boundary.

Figure 7 reveals a discontinuous interface between the asphalt and the grout material at the microscopic level. Two bright banded areas near the interface are noticeably different from the morphology of the grout material body, and the asphalt adjacent to the interface also shows significant variation from the asphalt body. In Figure 7(c), the area of the grout material close to the interface appears as a smooth, plate-like shape, presumed to be cement-asphalt (CA) mortar, indicating that the interface has hardened. Additionally, a large amount of $Ca(OH)_2$ aggregation is found near the grout material interface. Hexagonal $Ca(OH)_2$ is abundant in the ITZ near the grout material. The highly oriented $Ca(OH)_2$ crystals and their layered arrangement reduce bonding strength and increase susceptibility to cracking. Compared to hydrated calcium silicate (C-S-H) gel, the oriented $Ca(OH)_2$ contributes to a larger pore structure, which is detrimental in cement concrete (Zimbelmann 1985). The $Ca(OH)_2$ aggregation and oriented layering at the asphalt-grout ITZ compromise the integrity of the SFP composite material, resulting in a weak area on a macro scale.

Figure 8 shows the microscopic morphology of the ITZ between asphalt and three grout materials after interface enhancement. After the PAM specimens were immersed in a silane coupling agent and then grouting, the connection between the PAM specimens and the three cement-based grout materials was tighter compared with the original interface. Small cracks are present along the interface between the aggregate and asphalt, no cracks are visible at the junction of the grout and asphalt. The result demonstrates that the PAM specimens enhance the interface at the microscopic level after the interfacial modifier. This indicates that the connection performance of the grout material to the SFP composite interface is improved. The result shows that a large amount of bright material appears near the interface of the grout material. Although the use of interface modifiers can eliminate microcracks at the asphalt-grout ITZ, there is still a band-like area between the asphalt and the grout material that is different from the asphalt and the grout material. However, unlike the ordinary interface with two obvious bands, which merge into a wider band-like area after the reinforced interface.

3.4. Chemical components analysis

Line scanning EDS was conducted to scan the asphalt-grout ITZ of SFP, as shown in Figure 9. The samples without gold

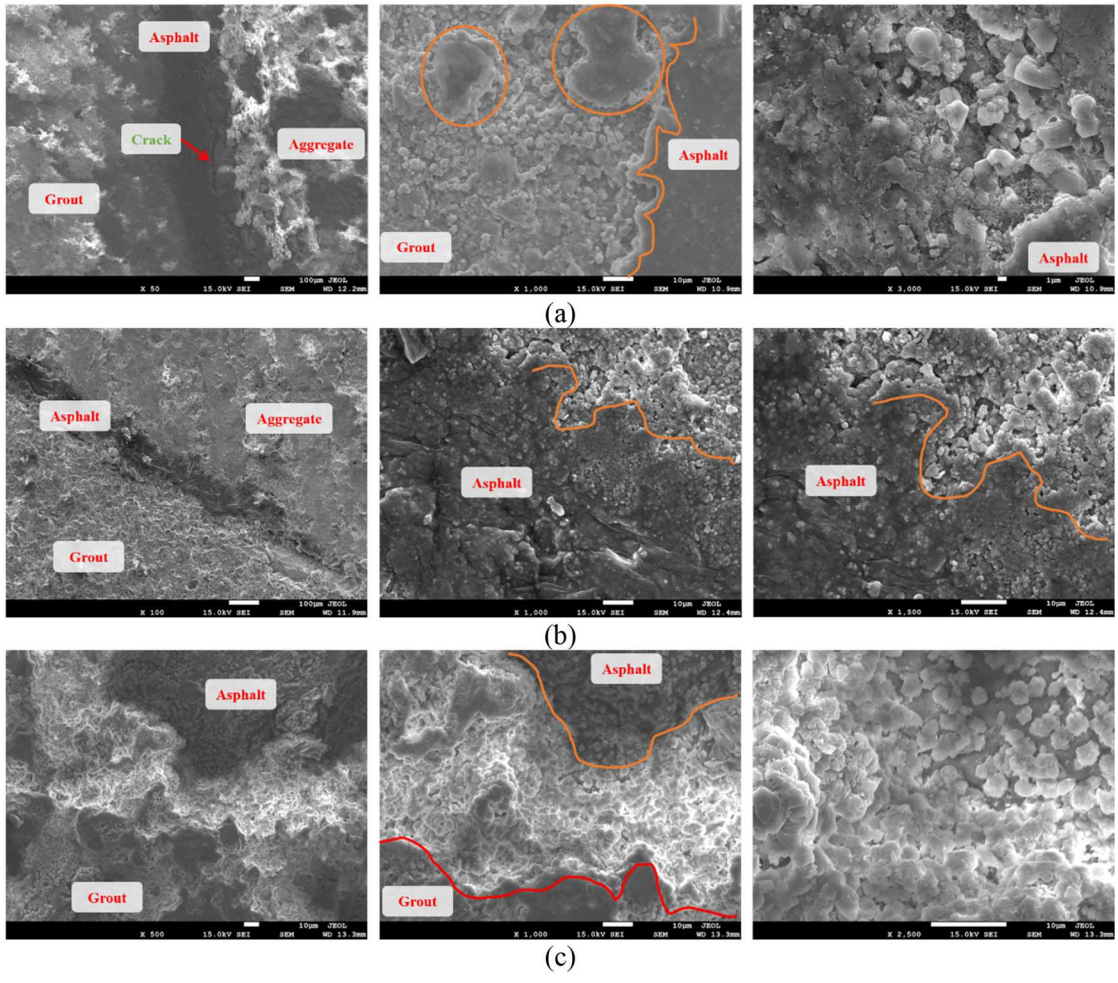

Figure 8. Microscopic morphology of the reinforced interface between asphalt and (a) GM-40, (b) GM-60, and (c) GM-70 grout materials in SFP. The red and yellow areas indicate the ITZ close to the grout and asphalt, respectively.

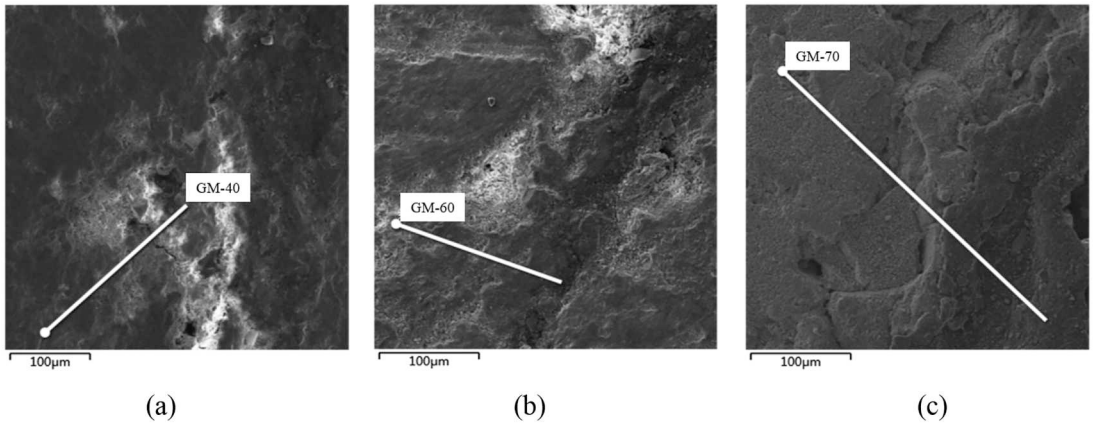

Figure 9. The EDS scan positions of the original interface between asphalt and (a) GM-40, (b) GM-60, and (c) GM-70 grout materials in SFP.

coating were used here since gold would influence the energy spectrum. Figure 10 shows the change in the amounts of elements across asphalt-grout phases. Note that only the areas near the asphalt-grout ITZ are shown. Figure 10 shows that the grout materials consist of more calcium (Ca) and oxygen (O) than the asphalt mastic. It is consistent with the limestone, which mainly consists of calcium carbonate and dioxide. A larger amount of carbon (C), together with sulfur (S) from asphaltene, can be found in asphalt mastic than the other two phases. It can also be found that the main products of cement-based grout after hydration are C-S-H gel, $Ca(OH)_2$, and calcium hydrate. The elements formed different material aggregations on both sides of the interface between asphalt and grout material. On the asphalt side, the aggregation peak area of Mg elements appeared mainly; on the grout side, the aggregation peak area of Ca elements appeared mainly.

The gaps with low element intensity can reflect the porous structure in asphalt-grout ITZ. The curves of the change in

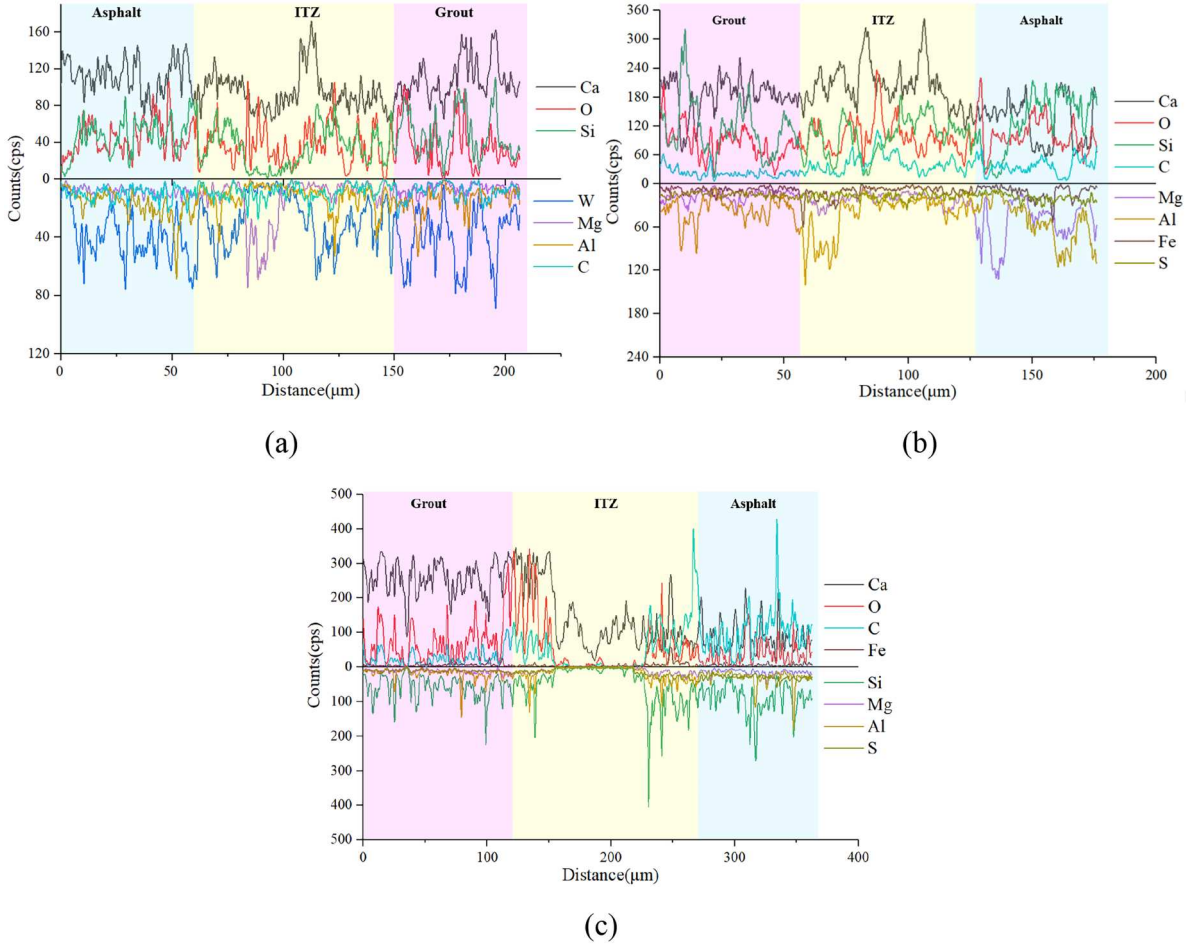

Figure 10. Chemical components of the original interface between asphalt and (a) GM-40, (b) GM-60, and (c) GM-70 grout materials in SFP.

elements of the asphalt-grout phase fluctuate markedly. The distribution of Fe and Al elements in Figure 10a is 80–120 μm, which is almost 0. At the same time, Figure 10c shows a cliff at 160–220 μm, that is, the element content is close to 0. This shows that there are tiny cracks between the asphalt and the grout material. Only the Ca element first decreases and then peaks in this area, indicating that $Ca(OH)_2$ will accumulate near the asphalt-grout interface on the grout side. Several high peaks are conspicuous in the curve of Ca. In the same region, the curves of O and Si present a gradual rise and the amounts of O are a little less than Si. It is compatible with the finding that Ca^{2+} tends to diffuse in the ITZ, resulting in the precipitation of $Ca(OH)_2$ in the ITZ oriented to the asphalt (Cai *et al.* 2020). Although the contents of Ca and O in the area near the grout material are less than those near the asphalt, the content of Si is much greater than that of O, indicating that more C-S-H is generated in the ITZ toward the cement paste, which is consistent with the SEM results. Therefore, it can be inferred that the thickness of ITZ between the asphalt and grout is around 100–170 μm.

Figure 11 shows the EDS scan positions of the reinforced interface between asphalt and different grout materials in SFP. The chemical components of the reinforced interface between asphalt and grout materials in SFP are shown in Figure 12. The results indicate that all elements are continuously distributed along the scanning line, with minimal fault areas. This confirms that immersing the PAM in a silane coupling agent solution and subsequently casting cement-based grout material to form SFP effectively improves the bonding performance of the composite interface. The immersion method introduces a layer of silane coupling agent at the asphalt-grout interface, resulting in a notable increase in the content of Si, O, and C elements, with a peak in C near the asphalt. Additionally, elements such as Mg, Al, Si, S, Ca, and Fe exhibit significant peaks at the grout materials, indicating their aggregation at this location. This suggests that the enhanced asphalt-grout interface maintains different elemental aggregations on both sides, preserving its double-layer structure after interface enhancement.

In comparison to the EDS results of a typical asphalt-grout interface, the enhanced interface shows no obvious fault areas along the scanning line. The distribution of elements is more continuous, and the transition between the two phases of asphalt and grout material is smoother. This further demonstrates the effectiveness of using a silane coupling agent solution to improve the bonding of the composite interface. Notably, the transition zone of the enhanced interface is slightly narrower than that of the common interface, measuring approximately 90–150 μm.

4. Discussions

4.1. Hydration products analysis

4.1.1. XRD analysis

In this subsection, the hydration products are detected using XRD and FTIR to analyze the phase composition of asphalt-grout ITZ. The XRD patterns of the hydration products at different grout materials are displayed in Figure 13. The $Ca(OH)_2$ produced by the hydration of grout materials, composed of cement, fine sand, and various additives, exhibits three distinctive diffraction peaks at 18.1°, 34.0°, and 47.0°. The $Ca(OH)_2$ absorption peak is notably present in GM-60 grout material after 28 days of hydration. At 34.0°, the main hydration products of ordinary cement, including $Ca(OH)_2$ and C–S-H, are observed (Bai *et al.* 2021). Calcium hydroxide constitutes about 20% of the solid phase of the hydrated slurry and tends to form large, unique hexagonal rhombic crystals. In GM-70, a decrease in SiO_2 content after hydration indicates that SiO_2 and $Ca(OH)_2$ undergo a secondary hydration reaction, resulting in no significant CH peak in its hydration products (Ergenç *et al.* 2020). In contrast, the composition of GM-40 differs markedly from that of GM-60 and GM-70, with calcium sulfate ($CaSO_4$) as the primary product after hydration.

4.1.2. FTIR analysis

The changes in the hydration products of different grout materials at 28 d hydration period are displayed in Figure 14. The transmission peaks of the three cement-based grout materials at high wavenumbers are similar, while slight differences are observed at low wavenumbers among GM-40, GM-60, and GM-70. This explains the distinct macroscopic

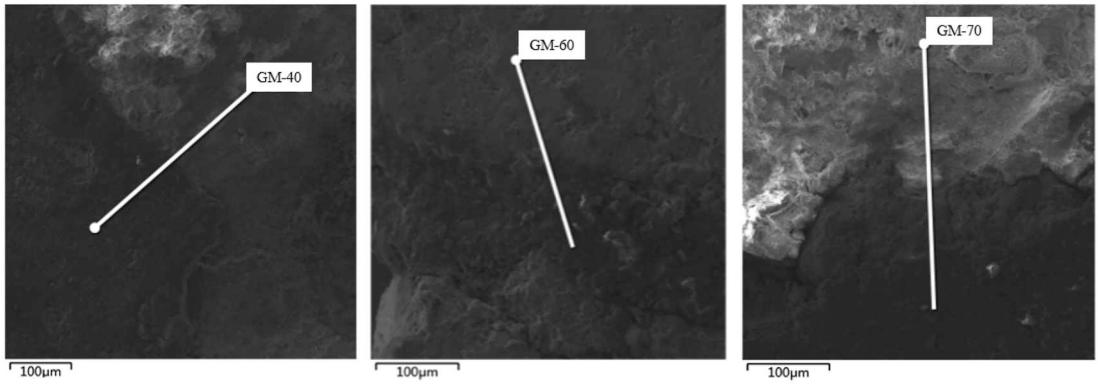

Figure 11. The EDS scan positions of the reinforced interface between asphalt and (a) GM-40, (b) GM-60, and (c) GM-70 grout materials in SFP.

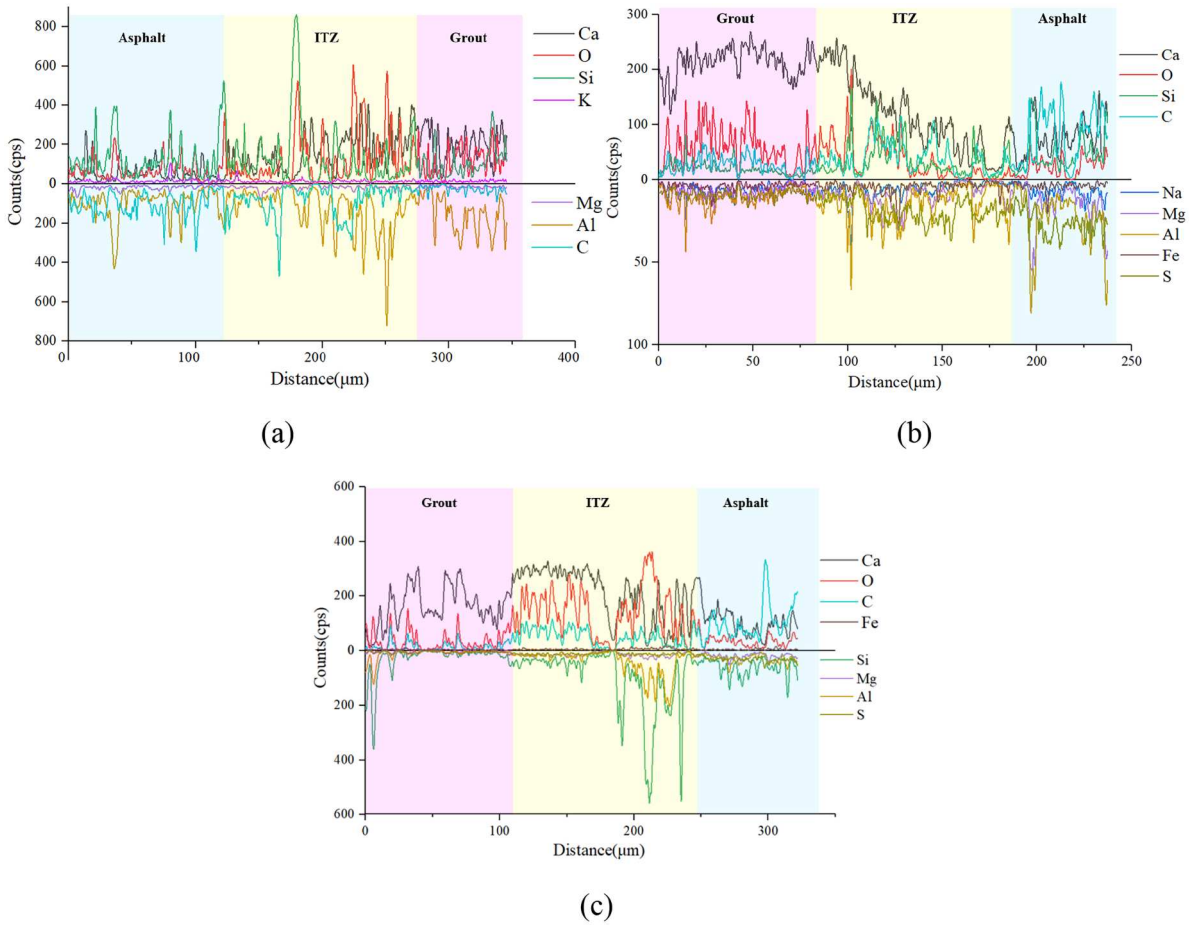

Figure 12. Chemical components of the reinforced interface between asphalt and (a) GM-40, (b) GM-60, and (c) GM-70 grout materials in SFP.

properties (strength, fluidity, *etc.*) of GM-40. The transmittance of the same absorption peak for GM-60 and GM-70 is comparable, indicating similar formulation components before hydration and consistent substances generated after hydration. However, the varying content of some substances may contribute to the differences in strength between the two grout materials.

In the range of 450 cm^{-1} to 490 cm^{-1}, the observed antisymmetric bending vibration corresponds to inactive silica (Si-O-Si), aligning with XRD analysis results. The peak around 874 cm^{-1} represents the out-of-plane bending vibration of carbonate ions (CO_3^{-2}), indicating the presence of calcium carbonate. At approximately 973 cm^{-1}, the Si-O stretching vibration is linked to the main tetrahedron in the hydrated slurry. The peak around 1647 cm^{-1} suggests O-H bending vibrations, likely from water, while the peak near 2925 cm^{-1} corresponds to H-C antisymmetric stretching vibrations. Finally, the peak around 3439 cm^{-1} also indicates O-H bending vibrations, further suggesting the presence of water.

4.2. Interfacial modification mechanism

In order to precisely regulate the bond strength at the interface between asphalt and cementitious grout, this study proposes to make the PAM specimens immersed in silane coupling agent solution and then grouted, which ensures that the silane coupling agent solution acts on the asphalt-grout ITZ as much as possible. The mechanism of the modified interface bonding effect between the grout material and the porous asphalt mixture is shown in Figure 15. Before interfacial modification, the gel surface of the grout material contains a large amount of free water and other substances in the grout slurry (unreacted slag, river sand, etc.), and the polarity of water and asphalt is opposite, which makes it difficult for the grout material to wet and contact with the porous asphalt mixture. Therefore, the bonding effect between the gel in the grout material and the porous asphalt mixture is poor. In contrast, after modification by the silane coupling agent, the hydrolysis process will generate silanol ($RSi(OH)_3$), where R is an organic group. These silanol can react with functional groups in asphalt (such as carboxyl, phenolic hydroxyl, etc.) to form stable covalent bonds. Subsequently, a large number of hydroxyl groups (-OH) will be generated after the hydration of cement-based grout materials. The hydroxyl groups in silanol can form hydrogen bonds with these hydroxyl groups or participate in chemical reactions. The reaction between hydroxyl groups may form new siloxane bonds (Si-O), enhancing the cross-linking degree of the material. At the same time, water molecules will be released during the reaction process, further promoting the hydration of the grout material and forming a more complex cross-linking network. The bonding effect between the grout material and the porous asphalt mixture is enhanced.

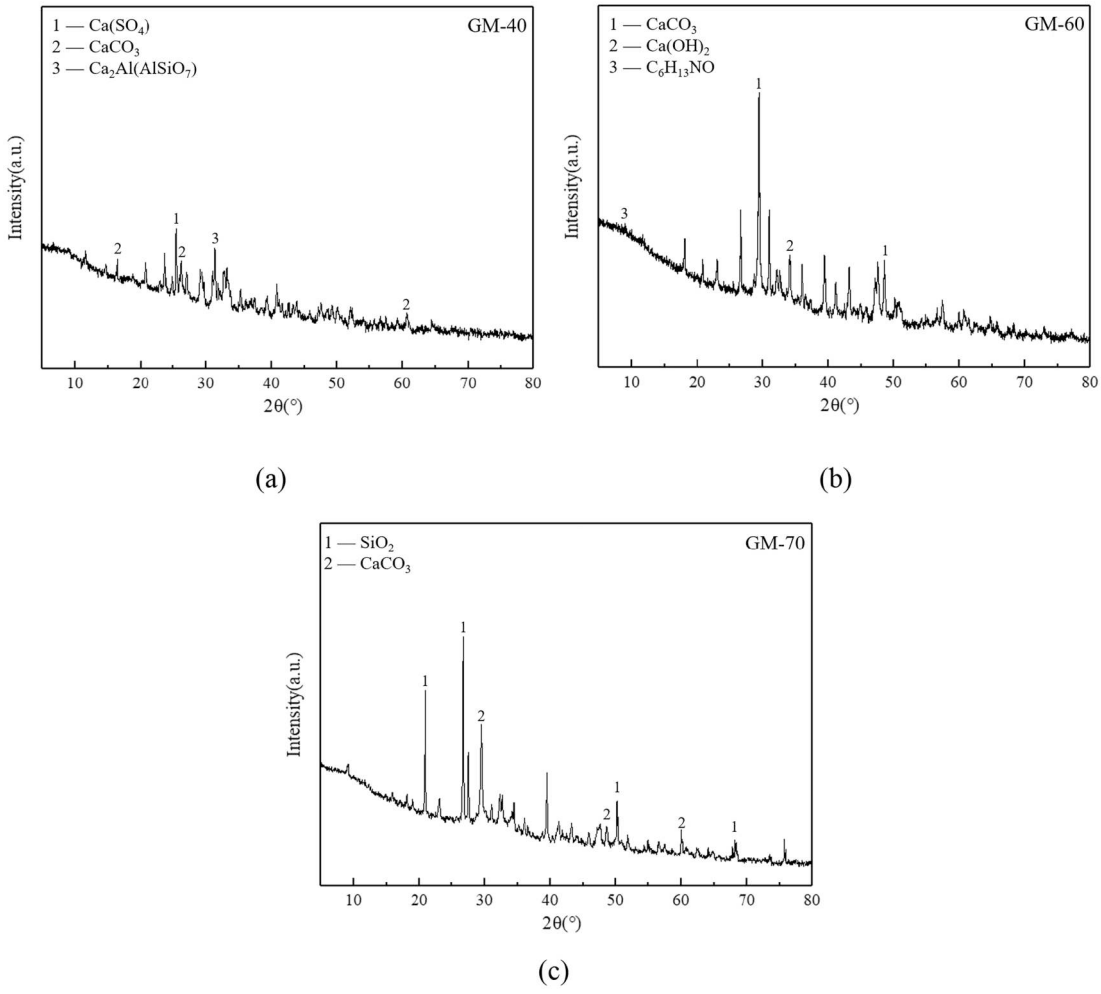

Figure 13. XRD patterns of hydration products for the grout materials: (a) GM-40, (b) GM-60, and (c) GM-70.

By comprehensively analyzing the SEM-EDS microstructure and elemental distribution maps of the asphalt-grout ITZ in SFP specimens prepared with three types of grouting materials of varying strengths before and after immersion in silane coupling agent solutions, it was observed that the silane coupling agent enhanced the bonding between inorganic cement-based grouting materials and organic asphalt. This improvement significantly enhanced the macroscopic mechanical performance of the SFP. Generally, the bonding performance between two materials in composite systems is closely related to the interactions at the microscopic level, which primarily occur in the interfacial transition zone (ITZ). The microstructural characteristics of this zone play a decisive role in the overall performance of composite materials. At the interface, both chemical and physical bonding typically exist, with chemical bonding having a more substantial impact on interfacial adhesion. In the SFP, the original interface between asphalt and cement-based grouting materials lacked chemical bonding. However, after treatment with the silane coupling agent solution, chemical bonds were formed at the interface, significantly improving the bonding strength between asphalt and cement-based grouting materials. Therefore, applying an interface modifier before pouring cement-based grout significantly enhances the microscopic bonding between asphalt and grout, reducing the likelihood of interface cracking and improving overall material integrity.

5. Conclusions

This paper aims to examine the microscopic morphology and chemical components of asphalt-grout ITZ in SFP material after an interfacial modifier. The asphalt-grout ITZ in SFP material is analyzed using a series of micromechanics techniques, including scanning electron microscopy (SEM) for microscopic morphology, energy dispersive spectrum analysis (EDS) for chemical components, X-ray diffraction (XRD) for phase composition, and Fourier-transform infrared spectroscopy (FTIR) for chemical bond information. The following conclusions were drawn from the analyses:

(1) The application of an interface modifier before the pouring of cement-based grout significantly improves the microscopic bonding between asphalt and grout. This modification reduces the likelihood of crack formation at the interface, contributing to enhanced material integrity.
(2) The asphalt-grout ITZ forms a double-layer structure at the microscopic level. Additionally, a high concentration

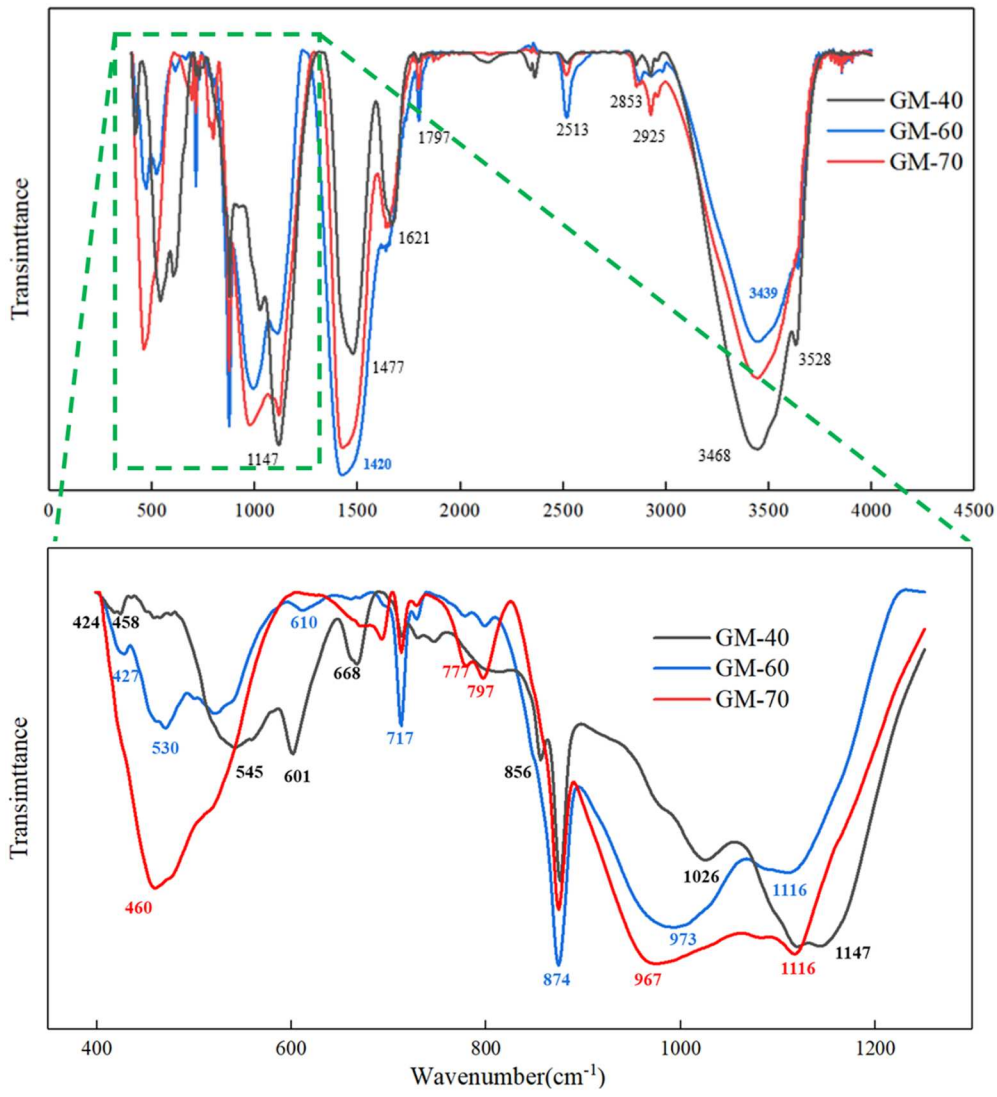

Figure 14. FTIR spectra of the different grout materials at 28 d hydration period.

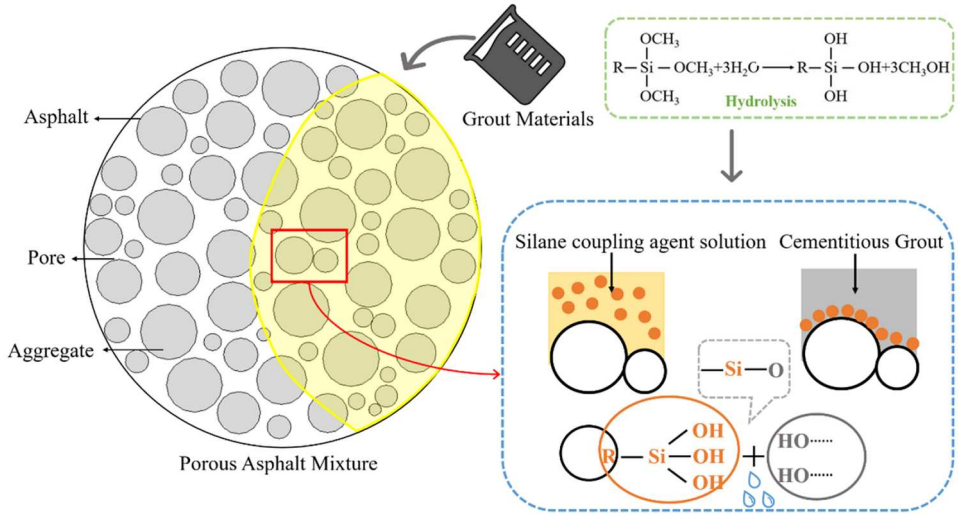

Figure 15. Illustration of the interface modification mechanism in the microstructure of SFP materials utilising a silane coupling agent.

of hexagonal $Ca(OH)_2$ crystals is observed near the interface, which is more prone to cracking compared to the more robust C–S-H gel.

(3) Post-enhancement, the distribution of elements at the asphalt-grout interface becomes more continuous, with smaller fluctuations compared to the untreated interface.

(4) The ITZ between asphalt and grout is significantly narrowed after the application of the interface modifier, in contrast to the untreated interface. This reduction in ITZ width further indicates the improvement in interface cohesion and material performance.

The research results elucidate how the microscopic morphology and chemical composition of asphalt-grout ITZ, provide theoretical support for the performance optimisation of SFP materials. Future work will explore the application of silane coupling agents in the construction of cold-mix SFP to mitigate the effects of elevated temperatures on their performance. Additionally, macroscopic tests will be conducted to evaluate the extent of degradation of silane coupling agents under highly alkaline cementitious environments.

Disclosure statement

No potential conflict of interest was reported by the author(s).

Funding

The work described in this paper is supported by the National Natural Science Foundation of China (No. 52338005, 51878193), and China Postdoctoral Science Foundation (No.2024M760619).

ORCID

Xiaoyu Liu http://orcid.org/0000-0003-4343-1591
Xu Cai http://orcid.org/0000-0001-6030-1137

References

Bai, R., *et al.*, 2021. Calcium hydroxide content and hydration degree of cement in cementitious composites containing calcium silicate slag. *Chemosphere*, 280, 130918.

Cai, X., *et al.*, 2020. Identification of microstructural characteristics in semi-flexible pavement material using micromechanics and nano-techniques. *Construction and Building Materials*, 246, 118426.

Cai, X., *et al.*, 2021. Identification of damage mechanisms during splitting test on SFP at different temperatures based on acoustic emission. *Construction and Building Materials*, 270, 121391.

Chen, Z., *et al.*, 2024. Research on cracking characteristics and failure modes of semi-flexible pavement materials. *Construction and Building Materials*, 452, 138915.

Cheng, P., Ma, G., and Li, Y., 2023. Preparation and performance improvement mechanism investigation of high-performance cementitious grout material for semi-flexible pavement. *Polymers (Basel)*, 15(12), 2631.

China, M.o.T.o.t.P.s.R.o., 2011. Standard test methods of bitumen and bituminous mixtures for highway engineering, People's Republic of China.

China, M.o.T.o.t.P.s.R.o., 2020. Test methods of cement and concrete for highway engineering, Industry Standard, People's Republic of China.

Davoodi, A., *et al.*, 2022. Influence of nano-silica modified rubber mortar and EVA modified porous asphalt on the performance improvement of modified semi-flexible pavement. *Construction and Building Materials*, 337, 127573.

Disfani, M.M., *et al.*, 2020. Performance evaluation of semi-flexible permeable pavements under cyclic loads. *International Journal of Pavement Engineering*, 21, 336–346.

dos Santos Ferreira, J.W., *et al.*, 2022. The feasibility of recycled micro polyethylene terephthalate (PET) replacing natural sand in hot-mix asphalt. *Construction and Building Materials*, 330, 127276.

Ergenç, D., *et al.*, 2020. Assessment on the performances of air lime-ceramic mortars with nano-Ca(OH)2 and nano-SiO2 additions. *Construction and Building Materials*, 232, 117163.

Fan, J., *et al.*, 2024. Interlayer failure characteristics of semi-flexible composite pavement structures (SFCPS) at high temperatures. *Construction and Building Materials*, 441, 137563.

Fang, Y., *et al.*, 2022. Synergistic effect of polycarboxylate superplasticizer and silica fume on early properties of early high strength grouting material for semi-flexible pavement. *Construction and Building Materials*, 319, 126065.

Gong, M., *et al.*, 2019. Evaluation on the cracking resistance of semi-flexible pavement mixture by laboratory research and field validation. *Construction and Building Materials*, 207, 387–395.

Hu, C., Zhou, Z., and Luo, Y., 2023. Study on damage evolution and mechanism of semi-flexible pavement under acid rain erosion. *Case Studies in Construction Materials*, 19, e02286.

Jiang, D., *et al.*, 2022. Research on the mesoscopic viscoelastic property of semi-flexible pavement mixture based on discrete element simulation. *Case Studies in Construction Materials*, 17, e01282.

Khan, M.I., *et al.*, 2022. Irradiated polyethylene terephthalate and fly ash based grouts for semi-flexible pavement: design and optimisation using response surface methodology. *International Journal of Pavement Engineering*, 23, 2515–2530.

Khan, M.N., *et al.*, 2024. Exploring waste marble dust as an additive in cementitious grouts for semi-flexible pavement applications: analysis and optimization using RSM. *Construction and Building Materials*, 411, 2515–2530.

Li, W., *et al.*, 2020. Study on the early cement hydration process in the presence of cationic asphalt emulsion. *Construction and Building Materials*, 261, 120025.

Li, G., *et al.*, 2022. Experimental study and performance characterization of semi-flexible pavements. *Coatings*, 12(2), 241.

Lin, Q., *et al.*, 2011. The reactivity of nano silica with calcium hydroxide. *Journal of Biomedical Materials Research Part B,* 99B, 239–246.

Ling, S., *et al.*, 2022. Pore characteristics and permeability simulation of porous asphalt mixture in pouring semi-flexible pavement. *Construction and Building Materials*, 330, 127253.

Ling, S., *et al.*, 2024. Predicting the mechanical properties of semi-flexible pavement material with micromechanical modeling. *Materials & Design*, 239, 112802.

Liu, X., *et al.*, 2023. Influence of the composite interface on the mechanical properties of semi-flexible pavement materials. *Construction and Building Materials*, 397, 132466.

Liu, X., *et al.*, 2025a. Numerical analysis of mechanical properties at the internal interface of SFP material using a digital image algorithm. *Materials and Structures*, 58(1), 43.

Liu, X., *et al.*, 2025b. Enhancing cracking resistance in semi-flexible pavements using an interfacial immersion method. *Case Studies in Construction Materials*, e04311.

Liu, X., *et al.*, 2025c. Microcosmic mechanism of reinforced interfacial transition zone in SFP materials: an insight from micro- and nano-scale tests. *Construction and Building Materials*, 481, 141521.

Montgomery, D.G., Hughes, D.C., and Williams, R.I.T., 1981. Fly ash in concrete – a microstructure study. *Cement and Concrete Research*, 11, 591–603.

Raza, M.S., and Sharma, S.K., 2024. A review of mechanical and durability properties and microstructure of semi-flexible pavement. *Innovative Infrastructure Solutions*, 9(4), 83.

Saboo, N., *et al.*, 2019. Optimal proportioning of grout constituents using mathematical programming for semi flexible pavement. *International Journal of Pavement Research and Technology*, 12, 297–306.

Song, J., *et al.*, 2024. Study on the improvement of fatigue and crack resistance of semi-flexible pavement materials using the mixing-molding method. *Construction and Building Materials*, 450, 138728.

Songqiang, C., *et al.*, 2024. Research on innovative preparation and performance of semi flexible pavement materials. *Case Studies in Construction Materials*, 20, e03050.

Su, K., Sun, L.-J., and Hachiya, Y., 2008. A new method for predicting rutting in asphalt pavements employing static uniaxial penetration test. *International Journal of Pavement Research and Technology*, 1, 24.

Sui, X., *et al.*, 2024. In-situ grouting rate prediction of semi-flexible pavement based on a novel composite dielectric constant model and ground-penetrating radar. *Construction and Building Materials*, 438, 137209.

Sun, Z., Hou, X.X., and He, G.P., 2015. Research on the crack resistance at low temperature and the mechanism of semi-flexible pavement. In: *International Conference on Chemical, Material and Food Engineering*, 533–536.

Tan, Q., *et al.*, 2024. Utilization of red mud in high-performance grouting material for semi-flexible pavement. *Journal of Cleaner Production*, 454, 142240.

Tian, Z., *et al.*, 2021. Potential using of water-soluble polymer latex modified greener road geopolymeric grouts: its preparation, characterization and mechanism. *Construction and Building Materials*, 273, 121757.

Wang, S., *et al.*, 2021. Fatigue resistance and cracking mechanism of semi-flexible pavement mixture. *Materials (Basel)*, 14(18), 5277.

Wang, Z., *et al.*, 2022. Laboratory investigation on pavement performance of indirect coal liquefaction residue in asphalt mixture. *Journal of Cleaner Production*, 363, 132183.

Wang, X., *et al.*, 2024. Random distribution of asphalt and cement mortar in semi-flexible pavement: implication for cracking resistance. *Construction and Building Materials*, 448, 138286.

Wu, K., *et al.*, 2021. Performance and fracture analysis of composite interfaces for semi-flexible pavement. *Coatings*, 11(10), 1231.

Xu, J., Kong, C., and Xu, T., 2021. Displacemental and mesomechanical responses of semi-flexible pavement based on discrete element method. *International Journal of Pavement Research and Technology*, 15(6), 1484–1497.

Yang, Y., *et al.*, 2011. The property research on interfacial modificated semi-flexible pavement material. *Applied Mechanics & Materials*, 71–78, 1090–1098.

Zarei, S., *et al.*, 2022a. Rutting and surface-initiated cracking mechanisms of semi-flexible pavements with cement asphalt emulsion pastes. *International Journal of Pavement Engineering*, 24(2), 2024187.

Zarei, S., Ouyang, J., and Zhao, Y., 2022b. Evaluation of fatigue life of semi-flexible pavement with cement asphalt emulsion pastes. *Construction and Building Materials*, 349, 128797.

Zhang, L., *et al.*, 2024a. Research on the crack resistance of semi-flexible pavement mixture based on meso-heterogeneous model. *Construction and Building Materials*, 411, 134495.

Zhang, M., *et al.*, 2024b. Multi-scale damage characterisation of semi-flexible pavements under freeze-thaw cycles. *Construction and Building Materials*, 445, 137847.

Zimbelmann, R., 1985. A contribution to the problem of cement-aggregate bond. *Cement and Concrete Research*, 15, 801–808.